frontiers | Frontiers in Earth Science

TYPE Original Research
PUBLISHED 19 August 2022
DOI 10.3389/feart.2022.978509



OPEN ACCESS

EDITED BY
Fei Ge,
Chengdu University of Information Technology, China

REVIEWED BY
Dachao Jin,
Nanjing University of Information Science and Technology, China
Xin Zhou,
Chengdu University of Information Technology, China

*CORRESPONDENCE
Kang Xu,
xukang@scsio.ac.cn
Weiqiang Wang,
weiqiang.wang@scsio.ac.cn

SPECIALTY SECTION
This article was submitted to Atmospheric Science, a section of the journal Frontiers in Earth Science

RECEIVED 26 June 2022
ACCEPTED 27 July 2022
PUBLISHED 19 August 2022

CITATION
Zhang X, Xu K, Wang W and He Z (2022), Revisiting the different responses of the following Indian summer monsoon rainfall to the diversity of El Niño events. *Front. Earth Sci.* 10:978509. doi: 10.3389/feart.2022.978509



# Revisiting the different responses of the following Indian summer monsoon rainfall to the diversity of El Niño events

Xiya Zhang[1,2], Kang Xu[1,3]*, Weiqiang Wang[1,3]* and Zhuoqi He[1,3]

[1]State Key Laboratory of Tropical Oceanography, South China Sea Institute of Oceanology, Chinese Academy of Sciences (CAS), Guangzhou, China, [2]University of Chinese Academy of Sciences, Beijing, China, [3]Southern Marine Science and Engineering Guangdong Laboratory (Guangzhou), Guangzhou, China

There is evidence that the interannual relationship between El Niño events and the following Indian summer monsoon rainfall (ISMR) has weakened with the more frequent occurrence of central Pacific (CP) El Niño events. We revisited the following ISMR responses to the two different types of El Niño events using observations and reanalysis datasets. Our results show that the ISMR anomalies associated with eastern Pacific (EP) and CP El Niño events are different, with decreased (increased) rainfall in early summer (June–July) following EP (CP) El Niño events. This is primarily attributed to the different responses to anomalous warming of the sea surface temperature (SST) in the northern Indian Ocean (NIO), which is characterized by double peaks in the warming SST during EP El Niño events, but only one peak during CP El Niño events. For EP El Niño events, the second SST warming peak in early summer contributes to the lower level antisymmetric wind pattern over the tropical Indian Ocean (TIO), which delays the onset of the Indian summer monsoon (ISM) and decreases the supply of moisture to India, implying a decrease in the ISMR. By contrast, for CP El Niño events, the cooling SST over the western TIO directly induces a significantly positive meridional SST gradient and drives the lower level southwesterly wind anomalies, resulting in an eastward shift in the decreased antisymmetric winds over TIO and the early onset of ISM. These circulation features are associated with anomalous upper-level divergence over TIO and sinking over India, jointly leading to the excess ISMR in early summer. These results suggest that, in addition to the key role of the warming of the NIO SST, cooling of the SST over the western TIO during CP El Niño events should be considered carefully in understanding the El Niño–ISMR relationship.

KEYWORDS

**eastern Pacific El Niño, central Pacific El Niño, Indian summer monsoon rainfall, northern Indian Ocean warming, antisymmetric wind pattern**

# 1 Introduction

The Indian summer monsoon rainfall (ISMR), which occurs in June–September (JJAS), is driven by the Indian summer monsoon (ISM; also known as the South Asian summer monsoon). The ISMR accounts for more than 75% of the total annual rainfall in India (Parthasarathy et al., 1994) and is crucially important to agricultural production and economic development over the subcontinent. As an important component of the global monsoon system, the ISM is characterized by strong southwesterly winds over the northern Indian Ocean (NIO) and the South Asian subcontinent in JJAS (Schott et al., 2009). However, due to the great uncertainty about the ISM and ISMR onset and intensity, it is challenging to accurately forecast for decades.

Previous studies have shown that the variability of ISMR can be linked to the activities of mid- and high-latitude systems (e.g., Krishnamurthy and Krishnamurthy, 2014; Malik et al., 2017) and coupled air–sea interactions in the tropics (e.g., Shukla and Paolino, 1983; Yang et al., 2007; Kucharski et al., 2008; Schott et al., 2009). Among these factors, the El Niño–Southern Oscillation (ENSO) is regarded as one of the most important on an interannual timescale, with the ENSO negatively (positively) correlating with the ISMR in its developing (decaying) phase (Mooley and Parthasarathy, 1983; Shukla and Paolino, 1983; Parthasarathy and Pant, 1985; Webster et al., 1998; Kumar et al., 2006). During the developing phase of El Niño events, the weakening and eastward shift in the Walker circulation anomalies caused by the warming sea surface temperature (SST) anomalies (SSTAs) in the tropical eastern and central Pacific induces significant anomalous sinking over the Indo-Pacific warm pool and suppress convective activities *in situ*, leading to a decrease in the ISMR (Shukla and Paolino, 1983). This is the so-called "atmospheric bridge" mechanism (Klein et al., 1999; Alexander et al., 2002; Lau and Nath, 2003).

El Niño events can also modulate the following ISM and its related ISMR anomalies by influencing the SSTAs in the tropical Indian Ocean (TIO; Terray et al., 2003; Park et al., 2010). El Niño events exert an impact on the anomalous warming of the SST in the southwestern Indian Ocean (SWIO) through the westward propagation of the downwelling ocean Rossby wave responses to the anomalous anticyclonic wind pattern over the tropical southeastern Indian Ocean induced by El Niño events (Xie et al., 2002; Xie et al., 2009). Such sustained warming of the SWIO causes south-trending SSTA gradients and induces a cross-equatorial antisymmetric pattern of atmospheric anomalies during the following spring and early summer (Xie et al., 2002; Wu et al., 2008; Wu and Yeh, 2010), which gives rise to a pronounced second warming peak in the SSTA over the NIO via a positive wind–evaporation–SST (WES) feedback mechanism (Du et al., 2009). These atmospheric circulations in the TIO inhibit the southwest ISM and reduce ISMR in early summer following El Niño events (Lü and Zheng, 2017). Park et al. (2010) found a greater number of rainfall anomalies over India in late summer following El Niño events through the "delayed effect" of these events.

However, the interannual relationship between El Niño events and the ISMR is unstable over the long term (Kripalani and Kulkarni, 1997) and has weakened since the 1990s (Kumar et al., 1999; Yang and Huang, 2021). This unstable relationship might be attributed to the more frequent occurrence of central Pacific (CP) El Niño events in recent decades (Kumar et al., 2006; Feba et al., 2021). In contrast with the conventional eastern Pacific (EP) El Niño events in which the warmest SSTA is centered in the eastern equatorial Pacific, CP El Niño events are primarily featured by the warmest SSTA in the central tropical Pacific and cooling SSTAs in the western and eastern tropical Pacific (Ashok et al., 2007; Kao and Yu, 2009; Ren and Jin, 2011; Xu et al., 2012; Xu et al., 2014; Capotondi et al., 2015; Xu et al., 2017; Xu et al., 2020).

EP and CP El Niño events have different impacts on the global climate (Ashok et al., 2007; Kug et al., 2009; Xu et al., 2013; Wang et al., 2019; Xu et al., 2019; Wang et al., 2021), including the Indian Ocean and surrounding regions (Kumar et al., 2006), presumably due to their distinct diabatic heating. For example, Tao et al. (2014) found that the weaker and more insignificant Indian Ocean basin mode (IOBM) is found in the following spring of CP El Niño events as a result of the absence of the tropospheric temperature mechanism and the related ocean dynamic process. Dogar et al. (2019) showed that CP El Niño events cause a decrease in the South Asian rainfall anomalies through modulation of the Hadley and Walker circulations, but these rainfall anomalies are weaker than that of EP El Niño events. Chowdary et al. (2017) also showed that the excess ISMR is mainly controlled by the rapid decay rate of the SSTAs in the TIO induced by CP El Niño events. In addition, Wang et al. (2013) emphasized that the late (early) onset of the Asian summer monsoon in the decaying years of EP (CP) El Niño events is determined by the significant (insignificant) warming of the southern Indian Ocean in the following spring. These evidence show the different impacts on the climate over the Indian Ocean associated with the two types of El Niño event, although the relationship between the variability of the ISMR and the diversity of El Niño events is not yet fully understood, especially the role of the anomalous SST in the TIO. Given the importance of the ISMR and the different impacts of the diversity of the El Niño on the climate in the Indian Ocean, we investigated whether ISMR shows different responses to these two types of El Niño event with the aim of clarifying the related physical mechanisms.

The remainder of the paper is organized as follows. The datasets and methods are briefly introduced in Section 2. Section 3 gives the main results of this study, including the different responses of the ISMR and the related atmospheric circulation anomalies, the role of the SSTA in the western NIO and the possible physical mechanisms. Our summary and discussion are presented in Section 4.

# 2 Data and methods

## 2.1 Data

The global monthly SST data was obtained from the Hadley Centre Sea Ice and Sea Surface Temperature (HadISST; Rayner et al., 2003) dataset with a horizontal resolution of 1° × 1°. Monthly three-dimensional wind datasets, which are available at a horizontal resolution of 2.5° × 2.5° and extend from 1000 to 10 hPa with 17 vertical pressure levels, were extracted from the United States National Center for Environmental Prediction–National Centers for Atmospheric Research (NCEP-NCAR) reanalysis products (Kalnay et al., 1996). Monthly rainfall data for all India were provided by the Indian Institute of Tropical Meteorology–Indian regional/subdivisional monthly rainfall (IITM-IMR; Parthasarathy et al., 1994) dataset. The anomaly in each variable was obtained by subtracting the climatological value from 1951 to 2016. All the monthly mean variables were linearly detrended and then smoothed by taking three-month running averages to exclude the subseasonal variability.

## 2.2 Classification of eastern Pacific and central Pacific El Niño events

Following the criterion of the NOAA, an El Niño event is defined by a three-month running Niño3.4 (5°S–5°N, 120°W–170°W) SSTA index greater than or equal to +0.5 K for at least five consecutive overlapping time periods. Because we mainly focused on moderate and stronger El Niño events, a total of 15 El Niño events were identified during the time period 1951–2016 (Table 1) based on peak values of the Niño3.4 SSTA greater than +1.0 K. We then determined the type of these selected El Niño events based on the consensus of three identification methods, including the Niño3/El Niño Modoki index (EMI) method of Ashok et al. (2007), the Niño3/Niño4 method of Yeh et al. (2009) and the EP/CP-index method of Kao and Yu (2009). Using the Niño3/EMI method, El Niño events were classified as central (eastern) Pacific types when the DJF mean EMI value was greater (less) than that of the Niño3 (5°S–5°N, 90°W–150°W) SSTA index. The EMI is defined as:

$$\mathrm{EMI} = [\mathrm{SSTA}]_c - 0.5[\mathrm{SSTA}]_E - 0.5[\mathrm{SSTA}]_W \quad (1)$$

where the square brackets with a subscript represent the area-averaged SSTA over the central (10°S–10°N, 165°E–140°W), eastern (15°S–5°N, 110°W–70°W) and western (10°S–20°N, 125°E–145°E) tropical Pacific, respectively.

TABLE 1 Major El Niño events during the time period 1951–2016 and their types identified by the majority consensus from the Niño3/Niño4 method, the EMI method and the EP/CP-index method.

| | El Niño years | Type | | | |
|---|---|---|---|---|---|
| | | Niño3/EMI index | Niño3/Niño4 index | EP/CP-index | Consensus |
| 1 | 1951–1952 | EP | EP | EP | EP |
| 2 | 1957–1958 | EP | CP | CP | CP |
| 3 | 1963–1964 | CP | CP | CP | CP |
| 4 | 1965–1966 | EP | EP | CP | EP |
| 5 | 1968–1969 | CP | CP | CP | CP |
| 6 | 1972–1973 | EP | EP | EP | EP |
| 7 | 1982–1983 | EP | EP | EP | EP |
| 8 | 1986–1987 | EP | EP | CP | EP |
| 9 | 1987–1988 | CP | CP | CP | CP |
| 10 | 1991–1992 | EP | EP | CP | EP |
| 11 | 1993–1994 | CP | CP | CP | CP |
| 12 | 1997–1998 | EP | EP | EP | EP |
| 13 | 2002–2003 | CP | CP | CP | CP |
| 14 | 2009–2010 | CP | CP | CP | CP |
| 15 | 2015–2016 | EP | EP | EP | EP |

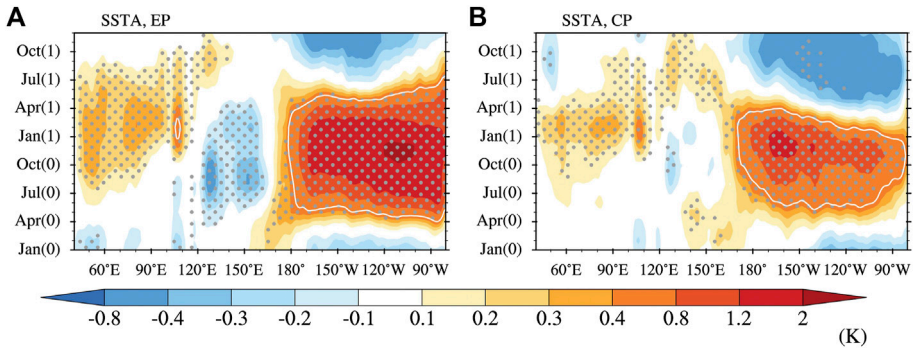


FIGURE 1
Time–longitude cross-section of the composite sea surface temperature anomaly (SSTA; units: K) at the equator (averaged from 5°S to 5°N) for **(A)** EP El Niño events and **(B)** CP El Niño events, where (0) indicates the El Niño developing year and (1) represents the decaying year. White contours indicate regions with a SSTA greater than +0.5 K and gray dots denote a SSTA statistically significant at the 90% confidence level.

With the Niño3/Niño4 method, El Niño events are classified as CP (EP) types when the DJF-averaged values of the Niño4 (5°S–5°N, 160°E–150°W) index are greater (less) than those of the Niño3 index.

Kao and Yu (2009) applied a combined regression–empirical orthogonal function (EOF) analysis to identify the EP and CP types of El Niño events and referred to this as the EP/CP-index method. In this method, El Niño events are classified as CP types when the DJF-averaged principal components of the EOF for the residual SSTA after removing the anomalies regressed with the Niño1+2 (0°–10°S, 80°W–90°W) SST index are greater than their counterparts after removing the anomalies regressed with the Niño4 index, and vice versa for the EP events. According to the majority consensus shown in Table 1, eight of the 15 major El Niño events were of the EP type and seven were of the CP type events.

# 3 Results

## 3.1 Contrasting responses of the Indian summer monsoon rainfall to the two types of El Niño event

To validate the rationality of the classification method for the two types of El Niño event used in this study, Figure 1 shows the temporal variation of the equatorial Indo-Pacific Ocean SSTA averaged between 5°S and 5°N associated with the EP and CP El Niño events. The center of the warming EP El Niño-related SSTA is observed in the eastern-central equatorial Pacific, with the warmest SSTA of +2.0 K to the east of 120°W (Figure 1A). By contrast, the significant anomalous SST warming during CP El Niño events shifts westward to the west of 150°W and its corresponding center with a maximum positive SSTA of +1.0 K is much weaker than that of the EP El Niño events (Figure 1B). Based on a significant SSTA greater than +0.5 K, a warm SSTA related to an EP (CP) El Niño event develops in April (June) of the developing year, peaks in winter and subsequently decays after the following June (April), indicating that the positive SSTA starts later and ends earlier during CP El Niño events, with a duration four months shorter and a decay rate much faster than for EP El Niño events.

Differences also exist in the strength and timing of the warming SSTA responses in the equatorial Indian Ocean to the two types of El Niño event. Anomalous equatorial Indian Ocean SST warming associated with EP El Niño events is stronger and lasts longer than that of CP El Niño events (Figure 1), highlighting the stronger IOBM and the subsequent air–sea interactions during EP El Niño events. This result indicates that EP El Niño events are followed by the IOBM until the following summer, but the warming SSTA related to CP El Niño events only lasts until the following spring and is insignificant in summer, consistent with the results of Tao et al. (2014). The classification method therefore effectively reflects the differences between EP and CP El Niño events, especially their different impacts on the SSTA in the equatorial Indian Ocean.

To investigate the different impacts of EP and CP El Niño events on rainfall anomalies over India, Figure 2 shows composites of the all-Indian rainfall anomalies during the decaying years of the two types of El Niño event. In the climatology, the ISMR in JJAS contributes as much as 75% to the annual rainfall over India, consistent with the results reported by Parthasarathy et al. (1994). It is clear that the larger standard deviations of the ISMR occur in JJAS (Figure 2, error bars), indicating that the ISMR also shows the most pronounced interannual variation. For the decaying years of EP El Niño, the ISMR shows a deficit in early summer

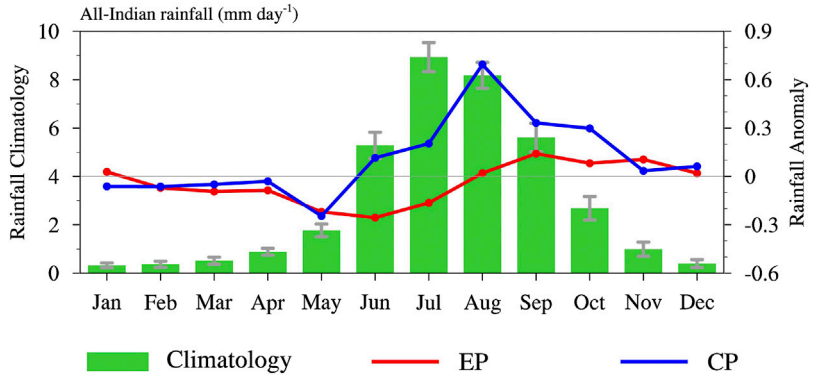


FIGURE 2
Climatology (1951–2016) of the all-India monthly rainfall (green bars; units: mm day$^{-1}$) and the anomalies (units: mm day$^{-1}$) of the all-India monthly rainfall during the decaying years of EP El Niño events (red) and CP El Niño events (blue). The gray error bars indicate one standard deviation.

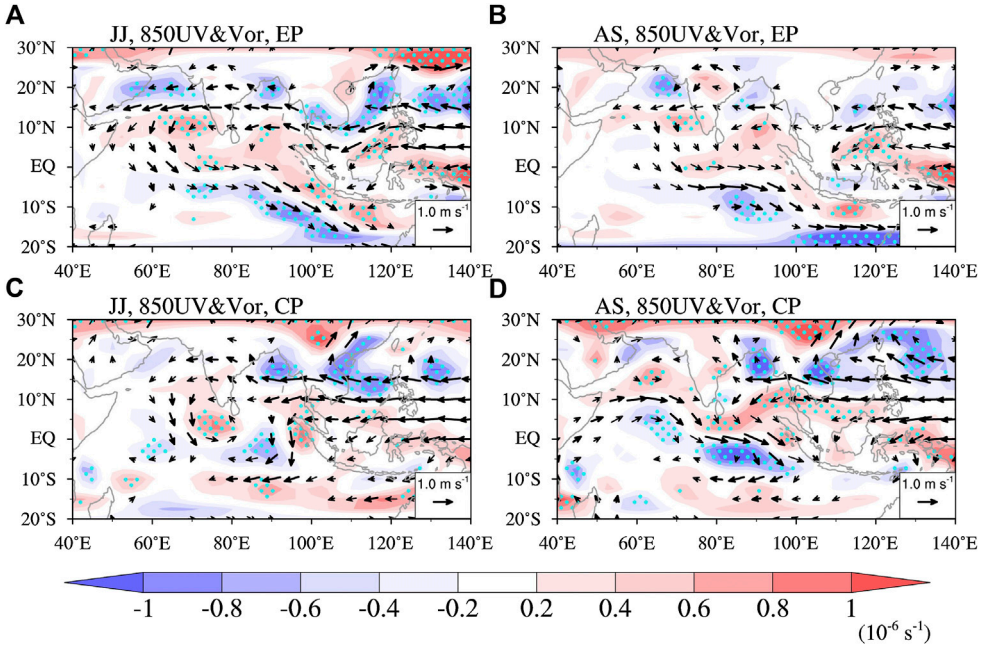


FIGURE 3
**(A)** June–July (JJ) and **(B)** August–September (AS) mean wind anomalies at 850 hPa (vectors; units: m s$^{-1}$) and their related relative vorticity anomalies (shading; units: $10^{-6}$ s$^{-1}$) for decaying EP El Niño events. **(C)** and **(D)** are the same as **(A)** and **(B)**, but for CP El Niño events. Only vectors with magnitudes greater than 0.2 m s$^{-1}$ are shown; cyan dots indicate relative vorticity anomalies above the 80% significance level.

(June–July), a surplus in late summer (August–September) and peaks in September, consistent with previous studies (Park et al., 2010; Lau and Nath, 2012; Lü and Zheng, 2017). By contrast, the ISMR is shows a greater surplus during the following JJAS of CP El Niño events and the peak in the ISMR anomalies occurs a month earlier than the peak in EP El Niño events.

The variations in the ISMR can be very different during the following JJAS, with suppressed (enhanced) rainfall in early summer for EP (CP) El Niño events (Figure 2). The opposite signs of the early summer rainfall over India associated with two the types of El Niño event imply that the corresponding onset time of the ISM also shows contrasting differences, with a late (early) onset of the ISM

for EP (CP) El Niño events. The responses of the ISMR to the two types of El Niño event are significantly different in early summer. The summer in El Niño decaying years is therefore divided into early (June–July, JJ) and late (August–September, AS) summer in the following analysis to explore the anomalous atmospheric circulation and SST and the related physical mechanisms.

## 3.2 Anomalous atmospheric circulation during the following summer for the two types of El Niño event

After inspecting the equatorial Indo-Pacific Ocean SSTAs related to the two types of El Niño event and their different impacts on the following ISMR, we investigated the associated atmospheric circulation anomalies over the tropics. Figure 3 shows the EP and CP El Niño composites of the 850 hPa winds and the relative vorticity anomalies in early and late summer. During the decaying years of EP El Niño events, an antisymmetric wind structure over the TIO is observed in early summer, with anomalous northeasterly flow to the north of the equator and anomalous northwesterly flow to the south of the equator (Figure 3A). Such an antisymmetric wind pattern is forced by the sustained warming of the SST over the SWIO associated with the El Niño-induced downwelling oceanic Rossby waves (Masumoto and Meyers, 1998; Du et al., 2009; Wu and Yeh, 2010). Anomalous northeasterly winds over the western NIO (WNIO) inhibit the southwest summer monsoon and reduce surface evaporation, thus delaying the onset of the ISM, leading to prominent warming of the SST over the NIO via the positive WES feedback (Xie and Philander, 1994). As a result of the westward expansion of the strong lower level easterlies over the NIO, less moisture is transported to South Asia and weak negative relative vorticity anomalies appear over the South Asian subcontinent (Figure 3A), which also reduce early summer rainfall over India (Figure 2). In late summer, however, the antisymmetric wind pattern is weakened and shifted eastward; weak westerly anomalies are observed over the WNIO (Figure 3B), indicating the start of the ISM. These warm and humid southwesterly winds substantially enhance the supply of moisture to South Asia and lead to stronger moisture convergence over India and significantly positive relative vorticity anomalies *in situ*, resulting in excess rainfall in this sector during the following AS season of the EP El Niño events.

During the early summer of the CP El Niño events, the lower level atmospheric circulation anomalies are similar to those for the late summer EP El Niño events, with an eastward shift of the weakened antisymmetric wind pattern over the TIO (Figure 3C). Significantly anomalous southwesterly winds over the WNIO cause the easterly anomalies to retreat eastward to the eastern Arabian Sea and then transport more moisture to South Asia. Significantly positive relative vorticity anomalies are also found over the south of the Indian subcontinent, leading to enhancement of the ISMR. This indicates that the ISM starts in JJ season when the onset time for the CP El Niño is about two months earlier than that for the EP El Niño. Two months later, anomalous southwesterly flow over the WNIO is gradually intensified and is more significant in AS season, along with the disappearance of the antisymmetric wind pattern over the TIO (Figure 3D). Over India, significant convergence of the relative vorticity anomalies and the increase in the amount of moisture transported by the anomalous southwesterly winds give rise to more rainfall *in situ* (Figure 2).

The velocity potential and divergence wind can be used to reflect the large-scale features of divergent motion (Tanaka et al., 2004). Figure 4 shows the differences between the velocity potential and divergence wind anomalies between 200 and 850 hPa in early and late summer related to EP and CP El Niño events. For the EP El Niño events, the most significant and strongest upper level convergence anomalies are centered over the western equatorial Pacific in early summer (Figure 4A), collocating with significantly negative local SSTAs (Figure 1A), whereas insignificant upper level divergence anomalies are located over the TIO (Figure 4A), along with the lower level antisymmetric wind pattern. In late summer, however, these upper level divergence anomalies are enhanced and are centered over the eastern TIO (Figure 4B). This divergent circulation indicates ascending motion over the TIO, which favors excess rainfall over India in AS season. By contrast, for CP El Niño events, the significant upper level divergence anomalies (and, by implication, ascending motion) in early summer are centered over the western TIO (Figure 4C), whereas the anomalies in late summer extend into the maritime continent and are progressively intensified (Figure 4D). Compared with the EP El Niño events, the most prominent difference in the upper level circulation related to CP El Niño events is the strong divergent anomalies over South Asia, which highlight the stronger ascending motion and higher rainfall during the following summer of CP El Niño events, especially in early summer. These results confirm the late onset of the ISM and lower ISMR in early summer for EP El Niño events, but a normal onset of the ISM and higher ISMR for CP El Niño events.

To further identify the possible connection between the ISMR and the local meridional cells associated with EP and CP El Niño events, Figure 5 shows composites of the latitude–height cross-sections of the wind and geopotential height anomalies averaged over India between 65 and 85°E. An anomalous clockwise circulation in early summer is observed over the Indian subcontinent for EP El Niño events (Figure 5A), with significant anomalous descending (ascending) motion over northern India (the TIO), suppressing convective activity over India and leading to less rainfall, despite the slightly converging anomalies of the water vapor flux (figure not shown). The upper level southerly wind and southward geopotential height gradient anomalies over India are also related to the

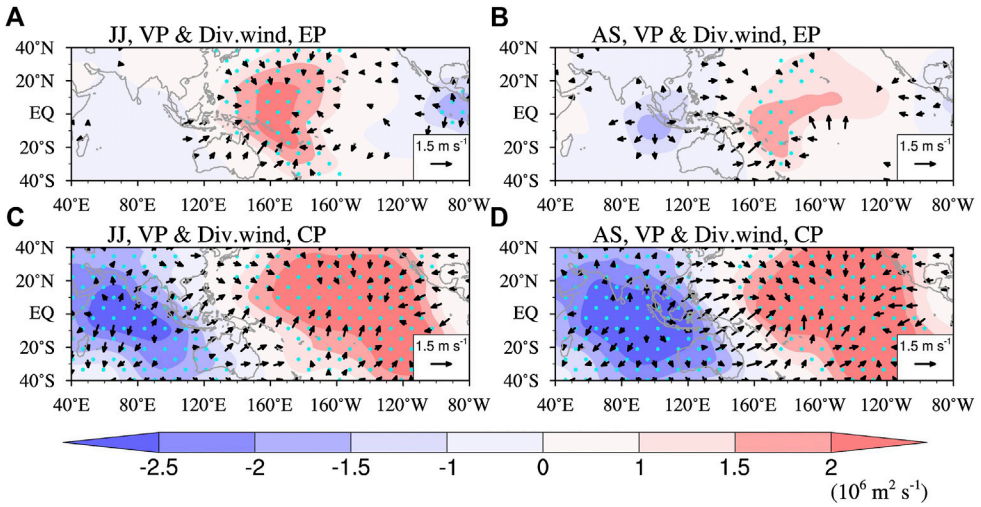


FIGURE 4
**(A)** June–July (JJ) and **(B)** August–September (AS) vertical shear of the divergence wind (vectors; units: $m^{-1}$) and velocity potential (VP, shading; units: 106 $m^2 s^{-1}$) anomalies between 200 and 850 hPa for decaying eastern Pacific (EP) El Niño events. **(C)** and **(D)** are the same as **(A)** and **(B)**, but for CP El Niño events. Only vectors with magnitudes greater than 0.2 m $s^{-1}$ are shown; cyan dots indicate relative vorticity anomalies above the 80% significance level.

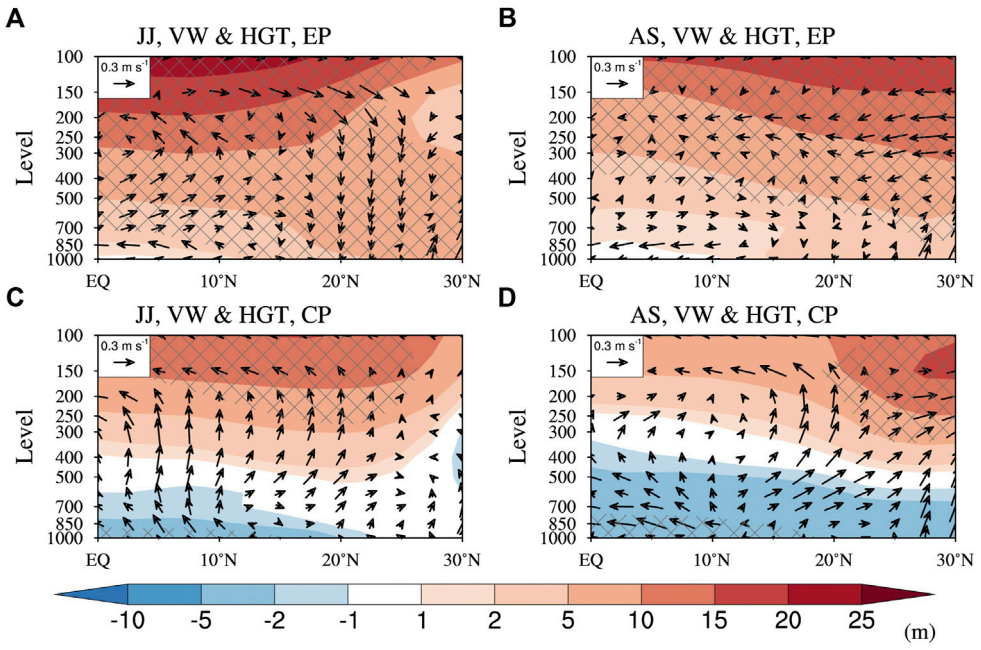


FIGURE 5
**(A)** June–July (JJ) and **(B)** August–September (AS) for the meridional circulation (vectors; units: m $s^{-1}$) and geopotential height (shading; units: m) anomalies averaged from 65 to 85° for decaying eastern Pacific (EP) El Niño events. **(C)** and **(D)** are the same as **(A)** and **(B)**, but for CP El Niño events. The vertical pressure velocity is multiplied by a factor of −50 for clarity. Gray crosses indicate geopotential height anomalies above the 80% significance level.

anomalous southwesterly winds, implying a delay and weakening of the ISM. Two months later, the significant anomalous sinking over northern India disappears and changes to ascending motion in the mid-troposphere from 300 to 500 hPa (Figure 5B). The inverted wind direction and geopotential height gradient indicate the occurrence of upper level northeasterly wind anomalies as well as the onset of the ISM, which both favor surplus rainfall in India in late summer.

By contrast, for CP El Niño events, significant anomalous ascending motion over India and the TIO are present in both early and late summer, along with upper level northerly wind anomalies, small lower level southerly wind anomalies (Figures 5C,D) and strong water vapor flux convergence anomalies (figure not shown). These types of circulation contribute to the onset of the ISM. The anomalous lower level southwesterlies with local convergence and ascending anomalies in late summer are stronger than those in early summer (Figures 5C,D). As a result, they can transport more moisture to India, enhancing the ISMR.

We have shown that the two types of El Niño event have different influences on the timing of the onset of the following ISM and ISMR. This is clearly due to the associated atmospheric circulation anomalies over the TIO in early summer. For EP El Niño events, India is influenced by anomalous easterlies related to the lower level antisymmetric wind pattern over the TIO, which delay the onset of the ISM and then suppress the transport of moisture to India, resulting in less-than-normal ISMR in early summer. By contrast, for the CP El Niño events, the enhanced southwesterly flow over the WNIO and weakened antisymmetric wind pattern over the TIO facilitate the onset of the ISM in early summer and also transport more moisture to South Asia. There is anomalous ascending motion over India, which boosts precipitation processes, leading to an increase in the ISMR.

## 3.3 Role of the sea surface temperature anomalies in the western northern Indian Ocean

Previous studies have shown that El Niño events can modulate the ISM via the subsequent warming of the SST in the TIO (Alexander et al., 2002; Lau and Nath, 2003; Du et al., 2009). We

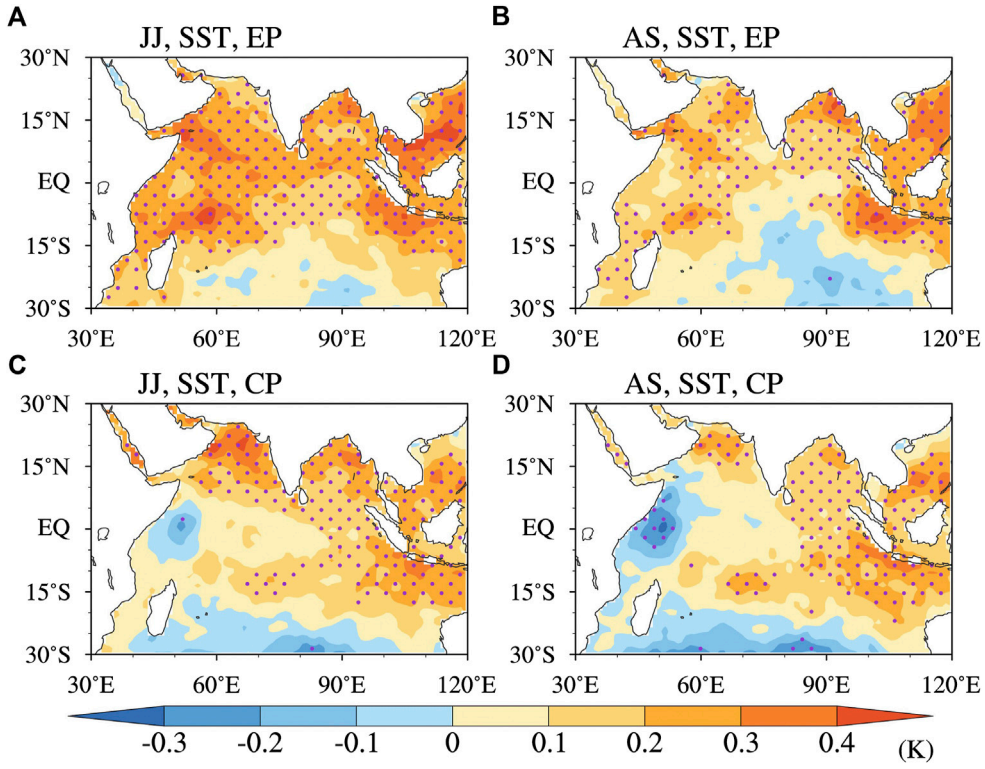


FIGURE 6
**(A)** June–July (JJ) and **(B)** August–September (AS) for the SSTA (units: K; shading) in the tropical Indian Ocean. **(C)** and **(D)** are the same as **(A)** and **(B)**, but for CP El Niño events. Purple dots indicate SSTA above the 80% significance level.

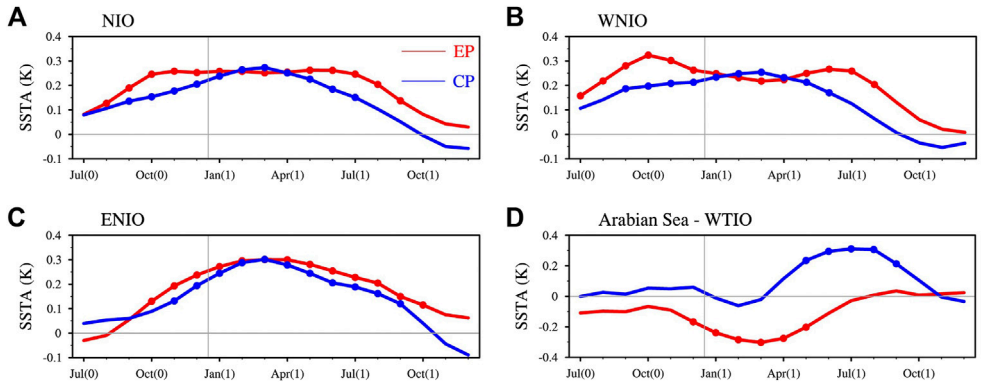


FIGURE 7
Monthly evolution of the sea surface temperature anomaly (SSTA; units: K) over **(A)** the northern Indian Ocean (NIO; 0–20°N, 50–100°E), **(B)** the western NIO (WNIO, 0–20°N, 50–80°E), **(C)** the eastern NIO (ENIO, 0–20°N, 80–100°E) during EP El Niño (blue) and CP El Niño (red) events. The time axis is from July of the El Niño developing year (0) to December of the following year (+1). Markers indicate signals statistically significant at the 90% confidence level. **(D)** Monthly evolution of the differences in the SSTA (units: K) between the Arabian Sea (15–25°N, 55–75°E) and the western TIO (WTIO, 10°S–10°N, 40–60°E).

also found remarkable differences in the strength and timing of the warming SSTA in the equatorial Indian Ocean in response to the two types of El Niño event (see Figure 1). We therefore further investigated the importance of the El Niño-associated SSTA patterns in the TIO in determining the atmospheric circulations in the TIO during the following summer of El Niño years (Figure 6).

During the early summer following EP El Niño events, the SSTA is characterized by the significantly warmer-than-normal temperature in the TIO, especially in the NIO (Figure 6A). This basin warming, which is the so-called second NIO SST warming (Du et al., 2009), can sustain an antisymmetric wind structure over the TIO with northeasterly (northwesterly) wind anomalies north (south) of the equator (see Figure 3A) via positive WES feedback. The significant southwestward SST gradient in the WNIO corresponds to the maintenance of an anomalous northeasterly flow, which, in turn, delays the onset of the ISM. Two months later, warming of the SST in the NIO gradually weakens in late summer (Figure 6B) and the positive SSTA in the WNIO decays faster and earlier than that in the eastern NIO (ENIO), corresponding to the weakening and eastward movement of the antisymmetric wind pattern over the TIO. This result indicates that the anomalous southwesterly flow transports more moisture to India and leads to excessive ISMR in late summer following EP El Niño events.

The largest difference in the SSTA pattern related to CP El Niño events compared with EP El Niño events is a significant cooling of the SSTA in the western TIO, highlighting a key role of the negative SSTA in the different responses of the ISMR to the two types of El Niño event. In early summer, significant warming of the SST is mainly concentrated in the NIO and the southeastern TIO, whereas a negative SSTA center is found along the eastern coast of Africa (Figure 6C). Both the warming SSTA in the Arabian Sea and the cooling SSTA in the western TIO form a positive meridional SSTA gradient in the WNIO, which can excite local southwesterly wind anomalies (see Figure 3C), contributing to the onset of the ISM. In AS season, the negative SSTA center along the coast of Africa is intensified and expanded, although warming of the SST in other regions is weakened (Figure 6D). The increased meridional SSTA gradient in the WNIO therefore continues to strengthen the southwesterly anomalies, which favors the increased transport of moisture to India and enhances the ISMR in late summer.

To further distinguish the relative role of the SSTA, we examined the El Niño composites for the monthly evolution of the SSTA in some key regions (Figure 7). It is clear that there are remarkably different responses of the SSTA in the NIO to different types of El Niño events. The warming of the SST over the NIO related to EP El Niño events (0–20°N, 50–100°E) is characterized by double peaks in the developing November and the following June, whereas the warming of the SST over the NIO related to CP El Niño events increases slowly with time and shows a single peak in the following March (Figure 7A). This result for CP El Niño events is inconsistent with the double warming of the NIO associated with El Niño events reported by Du et al. (2009).

The warming of the SST over the NIO in the following summer also shows a non-uniform zonal distribution in the two types of events (Figure 6). Significant double warming peaks are observed over the WNIO (0–20°N, 50–80°E) during EP El Niño events, but only a single warming peak during CP El Niño events (Figure 7B), consistent with the results for the NIO shown in Figure 7A. However, the responses of the SSTA over the ENIO (0–20°N, 80–100°E) to the two types of El Niño events show few

differences, with a single warming peak in the following March (Figure 7C). These results indicate that the warming SSTA in the WNIO makes a major contribution to the warming pattern of the SST in the NIO, whereas the counterpart in the ENIO has little effect.

Significantly different responses of the SSTA in the WNIO can result in different meridional SSTA gradients between the Arabian Sea (15–25°N, 55–75°E) and the western TIO (10°S–10°N, 40–60°E). As a result of the double warming peaks in the NIO associated with EP El Niño events, the negative meridional SSTA gradient persists from the winter to the following early summer (Figure 7D), which favors the maintenance of the northeasterly wind anomalies and leads to a delay in the onset of the ISM, suppressing ISMR in early summer. Until late summer, the meridional SSTA gradient changes from negative to slightly positive, heralding the onset of the ISM and an increase in the ISMR. By contrast, when the single warming peak related to CP El Niño events decays in early summer, the meridional SSTA gradient becomes positive and then remains significantly positive from the following May to September (Figure 7D), which corresponds to the anomalous southwesterly wind in the WNIO. This wind anomaly can contribute to the onset and intensification of the ISM, resulting in the enhanced ISMR. These analyses show that the different SSTAs in the WNIO associated with the two types of El Niño event are primarily attributed to the differences in the early summer ISMR anomalies between the EP and CP El Niño events.

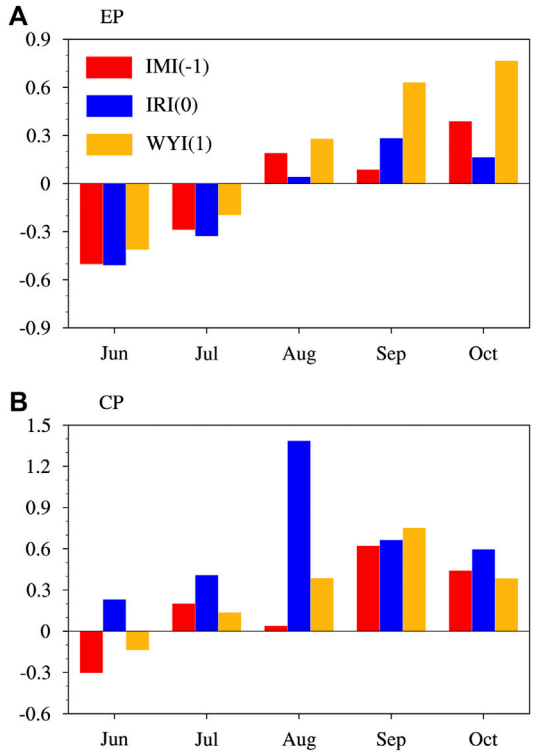


FIGURE 8
Composites of the monsoon indices for the decaying years of **(A)** EP and **(B)** CP El Niño events. IMI (−1), IRI (0) and WYI (1) represent the one-month-ahead Indian monsoon index, the simultaneous Indian rainfall index and the one-month-behind Webster–Yang index, respectively.

## 3.4 Possible physical mechanisms

We have considered the remarkable differences in the anomalous SST and atmospheric circulation patterns over the NIO associated with the two types of El Niño event. To investigate the possible physical mechanism of how the different SSTAs in the NIO might modulate the circulation related to the ISMR, we examined the monthly evolution of three groups of the ISM strength index in decaying years of the EP and CP El Niño events (Figure 8). The Indian monsoon index (IMI; Wang and Fan, 1999) is used to indicate the difference in the 850 hPa zonal wind between the southern Arabian Sea (5–15°N, 40–80°E) and the northern Indian continent (20–30°N, 70–90°E). The Indian rainfall index (IRI; Shukla and Paolino, 1983) refers to the standardized Indian rainfall, similar to the ISMR (shown in Figure 2) in this study. The Webster–Yang index (Webster and Yang, 1992) denotes the zonal wind shear between 850 and 200 hPa over the NIO (0–20°N, 40–110°E). The changes in these three indices from negative to positive represent the onset of the ISM. The IMI and the Webster–Yang index lead and lag the IRI, respectively (Figure 8), indicating that the onset of the ISM manifests first in the lower level zonal wind field, then in the rainfall over India and finally in the vertical shear of the zonal wind over the NIO.

For EP El Niño events, the second NIO SST warming peak in the following June (Figure 7A) induces the lower level antisymmetric wind over the TIO and its resultant northeasterly anomalies over the Arabian Sea inhibit the onset of the ISM, leading to a negative value of the simultaneous IMI. This lower level circulation decreases the transport of moisture and then gives rise to the negative IRI anomalies in early summer, which suppress the release of the heat of condensation over South Asia, resulting in negative zonal wind shear over the NIO in the following August (Figure 8A). By contrast, the single SST warming induced by CP El Niño events, which peaks in the following March, decays quickly during the late spring and summer (Figure 7A). The early summer SST cooling in the western TIO (Figure 6C) directly causes the significantly positive meridional SSTA gradient in the WNIO, which induces lower level southwesterly wind anomalies (Figure 3C), corresponding to the positive IMI in the following June and the onset of the ISM (Figure 8B). This lower level circulation can cause an eastward shift in the

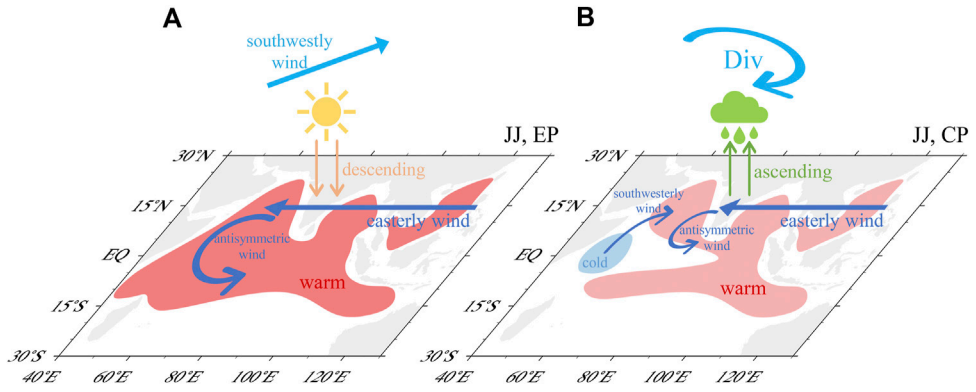


FIGURE 9
Schematic diagram illustrating the mechanism of the responses of the sea surface temperature anomaly in the northern Indian Ocean to **(A)** EP and **(B)** CP El Niño events and their effects on Indian summer monsoon rainfall in early summer (June–July) in decaying years.

decreased lower level antisymmetric wind over the TIO, which favors the onset of the ISM.

A comparison between EP and CP El Niño events suggests that the time of onset of the ISM circulation and the ISMR for CP El Niño events is about two months earlier than that of EP El Niño events. Anomalous ascending motion over India also enhances the positive IRI anomalies and the resultant release of the heat of condensation in early summer, leading to positive zonal wind shear over the NIO in the following July (Figure 8B). These results confirm that the different SSTA gradients in the WNIO attributed to the diversity of El Niño events can affect the time of onset of the ISM circulation in the early summer following the El Niño event and can therefore result in a deficit (surplus) in the ISMR associated with EP (CP) El Niño events.

## 4 Summary and discussion

Previous studies have shown a good correlation between the ISMR and ENSO on interannual scales, but this relationship has weakened since the 1990s, which might be attributed to the more frequent occurrence of CP El Niño events. We have revisited the interannual relationships of the ISMR with the diversity of El Niño events and examined its possible physical mechanism using observations and reanalysis datasets for the time period 1951–2016. Statistical analyses show that the ISMR has the most pronounced interannual variation and its responses to the decaying phase of EP and CP El Niño events show remarkable differences. In particular, the delay in the onset of the ISM and a reduced ISMR are found during the following early summer of EP El Niño events, whereas excess ISMR is observed in late summer. By contrast, there is excess ISMR in the summer following CP El Niño events and the related rainfall peak occurs 1 month earlier than for EP El Niño events. Further analysis showed that the warming of the SST in the NIO related to EP El Niño events is characterized by double peaks (mainly in WNIO but not in ENIO), but the warming related to CP El Niño events shows only a single peak. These differences primarily contribute to the differences in the early summer ISMR between EP and CP El Niño events. In addition, the WTIO cooling SSTA in CP El Niño plays a major contribution to the early onset of ISM circulation through generating the meridional SSTA gradient.

Figure 9 summarizes the SSTA and atmospheric responses over the NIO to EP and CP El Niño events and their influences on ISMR in the early summer of the decaying years. During early summer following an EP El Niño event, the second SST warming peak contributes to the lower level antisymmetric wind over the TIO via a positive WES feedback. The lower level northeasterly anomalies over the Arabian Sea caused by the antisymmetric wind pattern delay the onset of the ISM and therefore decrease the transport of moisture to South Asia, accompanied by upper level southwesterly anomalies and descending motion over India, ultimately resulting in a decrease in the ISMR (Figure 9A). By contrast, cooling of the SST in the western TIO and the rapid decay of the single warming peak of the SST in the NIO associated with CP El Niño events directly cause the significantly positive meridional SSTA gradient in the WNIO and drive the lower level southwesterly wind anomalies. This lower level circulation causes an eastward shift in the decreased antisymmetric wind over the TIO, which favors the onset of the ISM circulation. Both the upper level divergence anomalies over the TIO and the lower level southwest monsoon interact with each other and jointly induce anomalous ascending motion over India, leading to an increase in ISMR (Figure 9B).

These results suggest that a cold SSTA in the western TIO could be an important factor in modulating the ISMR anomalies related to CP El Niño events. However, details of its impact process or the remote teleconnection path by which CP El Niño events affect the SSTA in the western TIO have not been established. Tao et al. (2014) suggested that cooling of the SST in the eastern equatorial Pacific prevents the tropospheric temperature mechanism and the Rossby wave process from warming the SST in the TIO, leading to a weaker response of the SST to CP El Niño events. The response of the SST in the TIO to the diversity of El Niño events is complex and requires further investigation. It should be noted that, although the 1986–1987 El Niño event is classified as an eastern Pacific event in our classification, the following ISMR anomalies were strongly negative, differing from the composite results of the EP and CP El Niño events, which suggests that the ISMR may also be modulated by other factors. In addition, our results are based on statistical analyses with a small sample size and the possible physical mechanism of different responses of the ISMR to the diversity of El Niño events requires further modeling.

## Data availability statement

The original contributions presented in the study are included in the article/Supplementary Material, further inquiries can be directed to the corresponding authors.

## Author contributions

KX and WW conceived the idea and designed the study. XZ and KX processed and analyzed the datasets, performed the relevant statistical analysis, and wrote the first draft of the manuscript. All authors contributed to manuscript revision, read, and approved the submitted version.

## Funding

This work was jointly sponsored by the National Natural Science Foundation of China (42076020), the National Key R&D Program of China (2019YFA0606701), the Youth Innovation Promotion Association CAS (2020340), the Key Special Project for Introduced Talents Team of Southern Marine Science and Engineering Guangdong Laboratory (Guangzhou) (GML2019ZD0306), the Rising Star Foundation of the SCSIO (NHXX2018WL0201), and the Independent Research Project Program of LTO (LTOZZ2101).

## Acknowledgments

We would like to acknowledge the China-Sri Lanka Joint Center for Education and Research (CSL-CER), Chinese Academy of Science.

## Conflict of interest

The authors declare that the research was conducted in the absence of any commercial or financial relationships that could be construed as a potential conflict of interest.

## Publisher's note



## References

Alexander, M. A., Newman, M., Lanzante, J. R., Lau, N.-C., and Scott, J. D. (2002). Blade, IThe atmospheric bridge: The influence of ENSO teleconnections on air-sea interaction over the global oceans. *J. Clim.* 15 (16), 2205–2231. doi:10.1175/1520-0442(2002)015<2205:tabtio>2.0.co;2

Ashok, K., Behera, S. K., Rao, S. A., Weng, H., and Yamagata, T. (2007). El Niño Modoki and its possible teleconnection. *J. Geophys. Res.* 112 (C11), C11007. doi:10.1029/2006jc003798

Capotondi, A., Wittenberg, A. T., Newman, M., Lorenzo, E. D., Yu, J.-Y., Braconnot, P., et al. (2015). Understanding ENSO diversity. *Bull. Am. Meteorol. Soc.* 96 (6), 921–938. doi:10.1175/bams-d-13-00117.1

Chowdary, J. S., Harsha, H. S., Gnanaseelan, C., Srinivas, G., Parekh, A., Pillai, P., et al. (2017). Indian summer monsoon rainfall variability in response to differences in the decay phase of El Niño. *Clim. Dyn.* 48, 2707–2727. doi:10.1007/s00382-016-3233-1

Dogar, M. M., Kucharskib, F., Satoc, T., Mehmooda, S., Alia, S., Gongd, Z., et al. (2019). Towards understanding the global and regional climatic impacts of Modoki magnitude. *Glob. Planet. Change* 172, 223–241. doi:10.1016/j.gloplacha.2018.10.004

Du, Y., Xie, S.-P., Huang, G., and Hu, K. (2009). Role of air–sea interaction in the long persistence of El niño–induced north Indian Ocean warming. *J. Clim.* 22 (8), 2023–2038. doi:10.1175/2008jcli2590.1

Feba, F., Govardhan, D., Tejavath, C. T., and Ashok, K. (2021). "ENSO Modoki teleconnections to Indian summer monsoon rainfall—a review," in *Indian summer monsoon variability: El niño-teleconnections and beyond*. Editors J. S. Chowdary, A. Parekh, and C. Gnanaseelan (Amsterdam, Netherlands: Elsevier), 69–90.

Kalnay, E., Kanamitsu, M., Kistler, R., Collins, W., Deaven, D., Gandin, L., et al. (1996). The NCEP/NCAR 40-year reanalysis Project. *Bull. Am. Meteorol. Soc.* 77 (3), 437–471. doi:10.1175/1520-0477(1996)077<0437:tnyrp>2.0.co;2

Kao, H.-Y., and Yu, J.-Y. (2009). Contrasting eastern-pacific and central-pacific types of ENSO. *J. Clim.* 22 (3), 615–632. doi:10.1175/2008jcli2309.1

Klein, S. A., Soden, B. J., and Lau, N.-C. (1999). Remote sea surface temperature variations during ENSO: Evidence for a tropical atmospheric bridge. *J. Clim.* 12 (4), 917–932. doi:10.1175/1520-0442(1999)012<0917:rsstvd>2.0.co;2

Kripalani, R. H., and Kulkarni, A. (1997). Climatic impact of El Niño/La niña on the Indian monsoon: A new perspective. *Weather* 52 (2), 39–46. doi:10.1002/j.1477-8696.1997.tb06267.x

Krishnamurthy, L., and Krishnamurthy, V. (2014). Influence of PDO on South Asian summer monsoon and monsoon–ENSO relation. *Clim. Dyn.* 42, 2397–2410. doi:10.1007/s00382-013-1856-z

Kucharski, F., Bracco, A., Yoo, J. H., and Molteni, F. (2008). Atlantic forced component of the Indian monsoon interannual variability. *Geophys. Res. Lett.* 35 (4), L04706. doi:10.1029/2007gl033037

Kug, J.-S., Jin, F.-F., and An, S.-I. (2009). Two types of El Niño events: Cold tongue El Niño and warm pool El Niño. *J. Clim.* 22 (6), 1499–1515. doi:10.1175/2008jcli2624.1

Kumar, K. K., Rajagopalan, B., and Cane, M. A. (1999). On the weakening relationship between the Indian monsoon and ENSO. *Science* 284 (5423), 2156–2159. doi:10.1126/science.284.5423.2156

Kumar, K. K., Rajagopalan, B., Hoerling, M., Bates, G., and Cane, M. (2006). Unraveling the mystery of Indian monsoon failure during El Niño. *Science* 314 (5796), 115–119. doi:10.1126/science.1131152

Lau, N.-C., and Nath, M. J. (2012). A model study of the air–sea interaction associated with the climatological aspects and interannual variability of the south asian summer monsoon development. *J. Clim.* 25 (3), 839–857. doi:10.1175/jcli-d-11-00035.1

Lau, N.-C., and Nath, M. J. (2003). Atmosphere–ocean variations in the indo-pacific sector during ENSO episodes. *J. Clim.* 16 (1), 3–20. doi:10.1175/1520-0442(2003)016<0003:aoviti>2.0.co;2

Lü, L., and Zheng, X. (2017). The effect of Indian Ocean basin mode on Indian summer monsoon rainfall in decaying year of El Niño. *J. Trop. Oceanogr.* 36 (2), 1–11. doi:10.11978/2016054

Malik, A., Brönnimann, S., Stickler, A., Raible, C. C., Muthers, S., Anet, J., et al. (2017). Decadal to multi-decadal scale variability of Indian summer monsoon rainfall in the coupled ocean-atmosphere-chemistry climate model SOCOL-MPIOM. *Clim. Dyn.* 49, 3551–3572. doi:10.1007/s00382-017-3529-9

Masumoto, Y., and Meyers, G. (1998). Forced Rossby waves in the southern tropical Indian Ocean. *J. Geophys. Res.* 103 (C12), 27589–27602. doi:10.1029/98jc02546

Mooley, D. A., and Parthasarathy, B. (1983). Indian summer monsoon and El Niño. *pure Appl. Geophys.* 121 (2), 339–352. doi:10.1007/bf02590143

Park, H.-S., Chiang, J. C. H., Lintner, B. R., and Zhang, G. J. (2010). The delayed effect of major El Niño events on Indian monsoon rainfall. *J. Clim.* 23 (4), 932–946. doi:10.1175/2009jcli2916.1

Parthasarathy, B., Munot, A. A., and Kothawale, D. R. (1994). All-India monthly and seasonal rainfall series: 1871-1993. *Theor. Appl. Climatol.* 49, 217–224. doi:10.1007/BF00867461

Parthasarathy, B., and Pant, G. B. (1985). Seasonal relationships between Indian summer monsoon rainfall and the southern oscillation. *J. Climatol.* 5 (4), 369–378. doi:10.1002/joc.3370050404

Rayner, N. A., Parker, D. E., Horton, E. B., Folland, C. K., Alexander, L. V., Rowell, D. P., et al. (2003). Global analyses of sea surface temperature, sea ice, and night marine air temperature since the late nineteenth century. *J. Geophys. Res.* 108 (D14), 4407. doi:10.1029/2002jd002670

Ren, H.-L., and Jin, F.-F. (2011). Niño indices for two types of ENSO. *Geophys. Res. Lett.* 38 (4), L04704. doi:10.1029/2010gl046031

Schott, F. A., Xie, S.-P., and McCreary, J. P. (2009). Indian Ocean circulation and climate variability. *Rev. Geophys.* 47 (1), RG1002. doi:10.1029/2007rg000245

Shukla, J., and Paolino, D. A. (1983). The southern oscillation and long-range forecasting of the summer monsoon rainfall over India. *Mon. Weather Rev.* 111 (9), 1830–1837. doi:10.1175/1520-0493(1983)111<1830:tsoalr>2.0.co;2

Tanaka, H. L., Ishizaki, N., and Kitoh, A. (2004). Trend and interannual variability of Walker, monsoon and Hadley circulations defined by velocity potential in the upper troposphere. *Tellus A Dyn. Meteorology Oceanogr.* 56 (3), 250–269. doi:10.3402/tellusa.v56i3.14410

Tao, W., Huang, G., Hu, K., Qu, X., Wen, G., and Gong, Y. (2014). Different influences of two types of El Niños on the Indian Ocean SST variations. *Theor. Appl. Climatol.* 117, 475–484. doi:10.1007/s00704-013-1022-x

Terray, P., Delecluse, P., Labattu, S., and Terray, L. (2003). Sea surface temperature associations with the late Indian summer monsoon. *Clim. Dyn.* 21, 593–618. doi:10.1007/s00382-003-0354-0

Wang, B., and Fan, Z. (1999). Choice of South asian summer monsoon indices. *Bull. Am. Meteorol. Soc.* 80 (4), 629–638. doi:10.1175/1520-0477(1999)080<0629:cosasm>2.0.co;2

Wang, P., Tam, C.-Y., Lau, N.-C., and Xu, K. (2021). Future impacts of two types of El Niño on East Asian rainfall based on CMIP5 model projections. *Clim. Dyn.* 56 (3), 899–916. doi:10.1007/s00382-020-05510-0

Wang, P., Tam, C.-Y., and Xu, K. (2019). El Niño–East Asian monsoon teleconnection and its diversity in CMIP5 models. *Clim. Dyn.* 53 (9-10), 6417–6435. doi:10.1007/s00382-019-04938-3

Wang, X., Jiang, X., Yang, S., and Li, Y. (2013). Different impacts of the two types of El Niño on Asian summer monsoon onset. *Environ. Res. Lett.* 8 (4), 044053. doi:10.1088/1748-9326/8/4/044053

Webster, P. J., Magana, V. O., Palmer, T. N., Shukla, J., Tomas, R. A., Yanai, M., et al. (1998). Monsoons: Processes, predictability, and the prospects for prediction. *J. Geophys. Res.* 103 (C7), 14451–14510. doi:10.1029/97jc02719

Webster, P. J., and Yang, S. (1992). Monsoon and ENSO: Selectively interactive systems. *Q. J. R. Meteorol. Soc.* 118 (507), 877–926. doi:10.1002/qj.49711850705

Wu, R., Kirtman, B. P., and Krishnamurthy, V. (2008). An asymmetric mode of tropical Indian Ocean rainfall variability in boreal spring. *J. Geophys. Res.* 113, D05104. doi:10.1029/2007jd009316

Wu, R., and Yeh, S.-W. (2010). A further study of the tropical Indian Ocean asymmetric mode in boreal spring. *J. Geophys. Res.* 115, D08101. doi:10.1029/2009jd012999

Xie, S.-P., Annamalai, H., Schott, F. A., and McCreary, J. P. (2002). Structure and mechanisms of South Indian ocean climate variability. *J. Clim.* 15 (8), 864–878. doi:10.1175/1520-0442(2002)015<0864:samosi>2.0.co;2

Xie, S.-P., Hu, K., Hafner, J., Tokinaga, H., Du, Y., Huang, G., et al. (2009). Indian ocean capacitor effect on indo–western pacific climate during the summer following El Niño. *J. Clim.* 22 (3), 730–747. doi:10.1175/2008jcli2544.1

Xie, S.-P., and Philander, S. G. H. (1994). A coupled ocean-atmosphere model of relevance to the ITCZ in the eastern Pacific. *Tellus A Dyn. Meteorology Oceanogr.* 46 (4), 340–350. doi:10.3402/tellusa.v46i4.15484

Xu, K., Huang, R. X., Wang, W., Zhu, C., and Lu, R. (2017). Thermocline fluctuations in the equatorial pacific related to the two types of El Niño events. *J. Clim.* 30 (17), 6611–6627. doi:10.1175/jcli-d-16-0291.1

Xu, K., Liu, B., Liu, Y., Wang, W., and He, Z. (2019). Effects of monsoon onset vortex on heat budget in the mixed layer of the Bay of Bengal. *J. Oceanol. Limnol.* 38 (6), 1616–1631. doi:10.1007/s00343-019-9061-5

Xu, K., Su, J., and Zhu, C. (2014). The natural oscillation of two types of ENSO events based on analyses of CMIP5 model control runs. *Adv. Atmos. Sci.* 31 (4), 801–813. doi:10.1007/s00376-013-3153-5

Xu, K., Tam, C.-Y., Liu, B., Chen, S., Yang, X., He, Z., et al. (2020). Attenuation of central pacific El Niño amplitude by north pacific sea surface temperature anomalies. *J. Clim.* 33 (15), 6673–6688. doi:10.1175/jcli-d-19-0767.1

Xu, K., Zhu, C., and He, J. (2012). Linkage between the dominant modes in Pacific subsurface ocean temperature and the two type ENSO events. *Chin. Sci. Bull.* 57 (26), 3491–3496. doi:10.1007/s11434-012-5173-4

Xu, K., Zhu, C., and He, J. (2013). Two types of El Niño-related Southern Oscillation and their different impacts on global land precipitation. *Adv. Atmos. Sci.* 30 (6), 1743–1757. doi:10.1007/s00376-013-2272-3

Yang, J., Liu, Q., Xie, S.-P., Liu, Z., and Wu, L. (2007). Impact of the Indian Ocean SST basin mode on the Asian summer monsoon. *Geophys. Res. Lett.* 34 (2), L02708. doi:10.1029/2006gl028571

Yang, X., and Huang, P. (2021). Restored relationship between ENSO and Indian summer monsoon rainfall around 1999/2000. *Innovation* 2 (2), 100102. doi:10.1016/j.xinn.2021.100102

Yeh, S.-W., Kug, J.-S., Dewitte, B., Kwon, M.-H., Kirtman, B. P., and Jin, F.-F. (2009). El Niño in a changing climate. *Nature* 461, 511–514. doi:10.1038/nature08316